

## Different threshold and bipolar resistive switching mechanisms in reactively sputtered amorphous undoped and Cr-doped vanadium oxide thin films

Jonathan A. J. Rupp, Madec Querré, Andreas Kindsmüller, Marie-Paule Besland, Etienne Janod, Regina Dittmann, Rainer Waser, and Dirk J. Wouters

Citation: *Journal of Applied Physics* **123**, 044502 (2018); doi: 10.1063/1.5006145

View online: <https://doi.org/10.1063/1.5006145>

View Table of Contents: <http://aip.scitation.org/toc/jap/123/4>

Published by the [American Institute of Physics](#)

---

### Articles you may be interested in

[Effect of thermal insulation on the electrical characteristics of NbO<sub>x</sub> threshold switches](#)

*Applied Physics Letters* **112**, 073102 (2018); 10.1063/1.5015941

[A metal-insulator transition study of VO<sub>2</sub> thin films grown on sapphire substrates](#)

*Journal of Applied Physics* **122**, 235102 (2017); 10.1063/1.4997437

[NbO<sub>x</sub> based oscillation neuron for neuromorphic computing](#)

*Applied Physics Letters* **111**, 103503 (2017); 10.1063/1.4991917

[Analysis of the threshold switching mechanism of a Te–SbO selector device for crosspoint nonvolatile memory applications](#)

*Applied Physics Letters* **111**, 183501 (2017); 10.1063/1.4998493

[Light-activated resistance switching in SiO<sub>x</sub> RRAM devices](#)

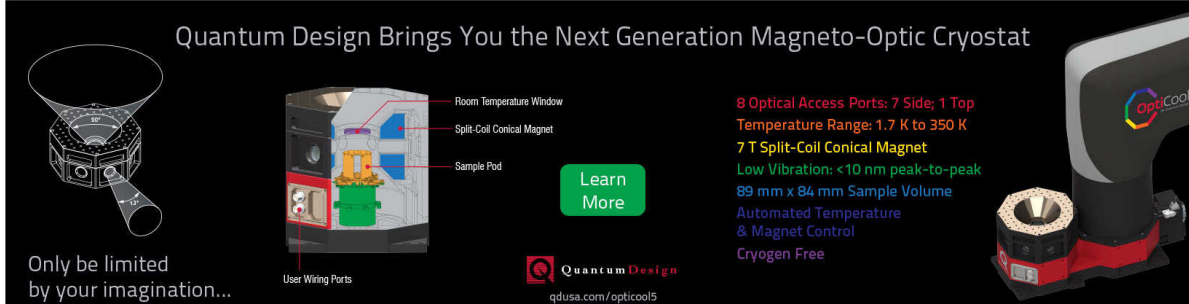
*Applied Physics Letters* **111**, 233502 (2017); 10.1063/1.5009069

[Irreversible metal-insulator transition in thin film VO<sub>2</sub> induced by soft X-ray irradiation](#)

*Applied Physics Letters* **111**, 241605 (2017); 10.1063/1.5012940

---

Quantum Design Brings You the Next Generation Magneto-Optic Cryostat



Only be limited by your imagination...

Learn More

Quantum Design  
qdusa.com/opticool5

8 Optical Access Ports: 7 Side; 1 Top  
Temperature Range: 1.7 K to 350 K  
7 T Split-Coil Conical Magnet  
Low Vibration: <10 nm peak-to-peak  
89 mm x 84 mm Sample Volume  
Automated Temperature & Magnet Control  
Cryogen Free

Room Temperature Window  
Split-Coil Conical Magnet  
Sample Pod  
User Wiring Ports

# Different threshold and bipolar resistive switching mechanisms in reactively sputtered amorphous undoped and Cr-doped vanadium oxide thin films

Jonathan A. J. Rupp,<sup>1,a)</sup> Madec Querré,<sup>2</sup> Andreas Kindsmüller,<sup>1</sup> Marie-Paule Besland,<sup>2</sup> Etienne Janod,<sup>2</sup> Regina Dittmann,<sup>3</sup> Rainer Waser,<sup>1,3</sup> and Dirk J. Wouters<sup>1,a)</sup>

<sup>1</sup>*Institut für Werkstoffe der Elektrotechnik II (IWE II), RWTH Aachen, Sommerfeldstraße 24, 52072 Aachen, Germany*

<sup>2</sup>*Institut des Matériaux Jean Rouxel (IMN), Université de Nantes, CNRS, 2 rue de la Houssinière, BP 32229, 44322 Nantes Cedex 3, France*

<sup>3</sup>*Forschungszentrum, Jülich PGI-7, 42425 Jülich, Germany*

(Received 22 September 2017; accepted 17 December 2017; published online 24 January 2018)

This study investigates resistive switching in amorphous undoped and Cr-doped vanadium oxide thin films synthesized by sputtering deposition at low oxygen partial pressure. Two different volatile threshold switching characteristics can occur as well as a non-volatile bipolar switching mechanism, depending on device stack symmetry and Cr-doping. The two threshold switching types are associated with different crystalline phases in the conduction filament created during an initial forming step. The first kind of threshold switching, observed for undoped vanadium oxide films, was, by its temperature dependence, proven to be associated with a thermally triggered insulator-to-metal transition in a crystalline VO<sub>2</sub> phase, whereas the threshold switch observed in chromium doped films is stable up to 90 °C and shows characteristics of an electronically induced Mott transition. This different behaviour for undoped versus doped films has been attributed to an increased stability of V<sup>3+</sup> due to the Cr<sup>3+</sup> doping (as evidenced by X-ray photoelectron spectroscopy analysis), probably favouring the creation of a crystalline Cr-doped V<sub>2</sub>O<sub>3</sub> phase (rather than a Cr-doped VO<sub>2</sub> phase) during the energetic forming step. The symmetric Pt/a-(V,Cr)O<sub>x</sub>/Pt device showing high temperature stable threshold switching may find interesting applications as a possible new selector device for resistive switching memory (ReRAM) crossbar arrays. *Published by AIP Publishing.* <https://doi.org/10.1063/1.5006145>

## I. INTRODUCTION

Electrically induced resistive switching phenomena, in particular in metal oxides, are of strong interest to develop novel devices enabling new types of memories and logic. Amongst many transition metal oxides that are subject of ongoing explorations, the complex material class of vanadium oxides spans a broad range with over 20 stable phases<sup>1</sup> which possess remarkable electrical switching properties. Most of the crystalline Magnéli V<sub>n</sub>O<sub>2n-1</sub> and Wadsley V<sub>n</sub>O<sub>2n+1</sub> phases show an Insulator-to-Metal transition (IMT)<sup>2</sup> below room temperature, while to our present knowledge there are only two well-established phases with an IMT above room temperature, namely VO<sub>2</sub> at 68 °C<sup>3</sup> and V<sub>3</sub>O<sub>5</sub> at 155 °C.<sup>4</sup> In the last decade, extensive research was carried out to exploit the electrical switching ability of VO<sub>2</sub> as a selector.<sup>5</sup> However, its applicability appeared seriously limited by its low transition temperature.<sup>6</sup> In addition, it has been shown that increasing Cr-content up to 11 at. % allows an increase of the IMT temperature of VO<sub>2</sub> by only about 11 °C.<sup>7</sup> An alternative is the use of NbO<sub>2</sub> with a much higher IMT temperature where the threshold switching was recently related to an electronic process rather than to the thermally triggered IMT itself.<sup>8</sup> Moreover, the Cr-doped V<sub>2</sub>O<sub>3</sub> phase is well known as the archetype of Mott insulators,<sup>9</sup> in which an electric-field-driven volatile resistive switching can be

established by triggering of the Mott transition via an electronic (avalanche breakdown) mechanism.<sup>10</sup> Apart from these specific IMT- and Mott-phase associated resistive change phenomena, we may expect a non-volatile resistive switching mechanism based on a valence change (VCM) by the drift of oxygen vacancies, which is a general observed process in transition metal oxides.<sup>11</sup> All mentioned mechanisms can in theory take place in Cr-doped vanadium oxides depending on which conditions and crystalline phases come into play. In this paper, we report on a systematic investigation of the switching behaviour of low oxygen content (V:O ~ 2:3, i.e., close to V<sub>2</sub>O<sub>3</sub>) amorphous VO<sub>x</sub> and (V,Cr)O<sub>x</sub> thin films deposited by reactive physical vapor deposition process (PVD) using both symmetric and asymmetric metal-insulator-metal (MIM) structures. We show that, after an energetic forming process, different threshold and bipolar resistive switching (BRS) mechanisms occur depending on the material (Cr doped or undoped) and choice of the electrode material (Pt or V top electrode). These results might be understood by the formation of different crystalline material phases within a switching filament.

## II. EXPERIMENTAL DETAILS

Amorphous undoped and Cr-doped VO<sub>x</sub> films with a thickness of 90 nm have been deposited by reactive RF magnetron sputtering at room temperature with a growth rate of 6.3 nm/min. A one inch metallic vanadium target was used

<sup>a)</sup>rupp@iwe.RWTH-Aachen.de and wouters@iwe.RWTH-Aachen.de

with a power of  $P_V=100$  W, while (for the Cr-doped films) Cr was co-sputtered (with a power of  $P_{Cr}=5-10$  W) from a one inch metallic Cr-target. The distance between target and substrate constituted 5 cm. As determined by X-ray Photoelectron Spectroscopy (XPS) measurements, the Cr-doping level was 3 at. % Cr for 5 W and 10 at. % for 10 W sputter power—(see [supplementary material](#) Table S1). The base pressure was held below  $p_{base}<1$  nbar and the process pressure was fixed at  $p_{process}=10$   $\mu$ bar. The oxygen flow was introduced close to the target. Hereby, the oxygen partial pressure  $p(O_2)$  was adjusted by the flux ratio of two mass flow controllers: one with pure argon (90 sccm) and one with a mixture of argon and oxygen in the ratio 99:1 (10 sccm). This allowed the control of the  $p(O_2)$  in a few 10 nbar range. The relatively low oxygen partial pressure value of 10 nbar was used to target a V:O ratio in the amorphous film close to 2:3. Indeed, a separate (unpublished) study by the authors of the deposition of crystalline (Cr)VO<sub>x</sub> films at high temperature up to 600 °C showed the desired V<sub>2</sub>O<sub>3</sub> phase at this pressure. High-temperature deposited crystalline films were also used as XPS reference samples. Thin film morphology was investigated by Scanning Electron Microscopy (SEM) with a Zeiss “DSM982 GEMINI;” roughness of thin films was calculated out of  $1 \times 1 \mu m^2$  area scans using Atomic Force Microscopy (AFM) measurements performed with a Veeco “di CP II”. Density and thickness of thin films were extracted from the X-ray Reflectivity (XRR) measurements obtained with an X-Ray Diffractometer from PANalytical “X’Pert PRO”. The different oxidation states of thin films were determined from XPS analysis using a “PHI 5000 Versa Probe II” of Ulvac-Phi, Inc. XRR fitting was performed by PANalytical’s “X’pert Reflectometry” and XPS fitting by “CasaXPS” v2.3.17. Crystallinity was probed by X-ray diffraction in surface sensitive grazing incidence mode (XRD-GI).

For all analysis, undoped and Cr-doped VO<sub>x</sub> films were deposited on a 30 nm thick Pt electrode on SiO<sub>2</sub>/Si substrates with a 5 nm Ti sticking layer in between SiO<sub>2</sub> and Pt. To prevent layer oxidation of samples for XPS analysis, films were capped *in situ* with 50 nm of sputtered Au and transported to the XPS system where the Au cap was removed inside the vacuum system just before analysis. Study of the resistive switching properties of amorphous undoped and Cr-doped VO<sub>x</sub> thin films was performed by using symmetric as well as asymmetric MIM devices (Figs. 3 and 4). For MIM devices, a 100 nm thick Pt or a stacked (50 nm V/50 nm Pt) electrode was used on top of (V,Cr)O<sub>x</sub> thin films. Devices were patterned by UV-lithography and lift-off processes.

Electrical characterization was performed by quasistatic  $I$ - $V$  measurements from room temperature up to 90 °C on  $10 \times 10 \mu m^2$  and  $25 \times 25 \mu m^2$  pads which showed similar behaviour. Here, we report on  $25 \times 25 \mu m^2$  devices. The voltage was imposed on the top electrode whereas the bottom electrode was held on ground potential.

### III. RESULTS

#### A. Layer morphology

As a representative example for all investigated amorphous layers, SEM, AFM and fitted XRR-analysis for

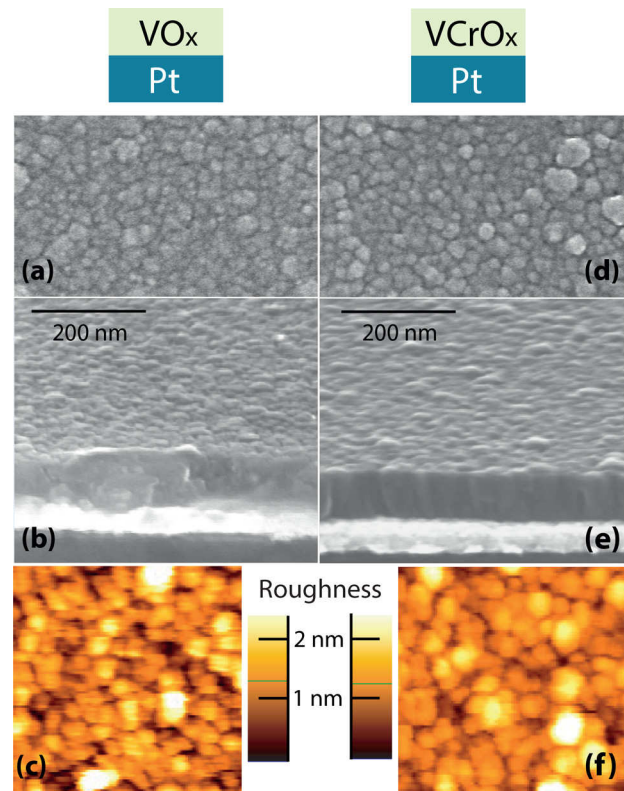


FIG. 1. SEM plan view and cross section images of 90 nm thick VO<sub>x</sub> [(a) and (b)] and (V<sub>0.97</sub>Cr<sub>0.03</sub>)O<sub>x</sub> [(d) and (e)] thin films deposited on 30 nm Pt. One can see the same surface roughness but an oriented columnar grain growth and a higher density for Cr-doped VO<sub>x</sub>. Bottom part: Topography of VO<sub>x</sub> (c) and (V<sub>0.97</sub>Cr<sub>0.03</sub>)O<sub>x</sub> (f) thin films determined by AFM with roughness as false color scale.

undoped and Cr-doped low oxygen content (V:O  $\sim$  2:3) VO<sub>x</sub> films are given in Fig. 1 and Table I.

As displayed, the undoped VO<sub>x</sub> film exhibits a porous microstructure [Fig. 1(a)] with a random grain orientation in cross section [Fig. 1(b)] and a density of 4.0 g/cm<sup>3</sup>, calculated by XRR-fitting (Table I). In contrast, the Cr-doped layer/films (V,Cr)O<sub>x</sub> show a denser and vertically aligned columnar structure where some grain edges emerge out of the surface plane [Fig. 1(d)] and with low inter-columnar spaces [Fig. 1(e)]. The higher density is supported by a higher XRR-fitted density of 4.4 g/cm<sup>3</sup> (Table I). The mean square roughness extracted from AFM images [Figs. 1(c) and 1(f)] and XRR-fitting (Table I) is similar in the 1.3 to 1.5 nm range for both samples.

#### B. Oxidation state

To evaluate the oxidation states of amorphous layers, XPS spectra of V<sub>2p</sub> core level spectra were measured for both undoped and 10 at. % Cr-doped VO<sub>x</sub> sputtered amorphous thin films (Fig. 2). The relatively high Cr-content was

TABLE I. Thickness  $d$ , density  $\rho$ , and mean square roughness  $R_{ms}$  extracted from XRR/AFM measurements and fit data.

Material	$d$ (nm)	$\rho$ (g/cm <sup>3</sup> )	$R_{ms}$ (nm) (XRR)	$R_{ms}$ (nm) (AFM)
VO <sub>x</sub>	$89 \pm 2$	$4.0 \pm 0.1$	$1.5 \pm 0.1$	$1.3 \pm 0.2$
VCrO <sub>x</sub>	$90 \pm 1$	$4.4 \pm 0.1$	$1.3 \pm 0.1$	$1.2 \pm 0.2$

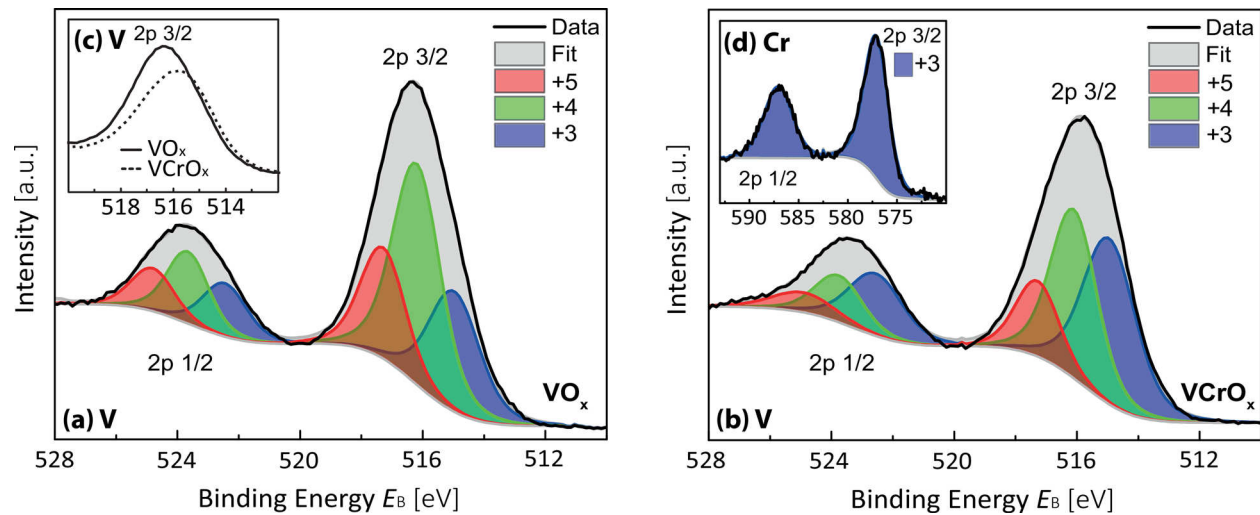


FIG. 2. Vanadium  $V_{2p}$  core level spectra of amorphous  $VO_x$  (a) and  $(V_{0.9}Cr_{0.1})O_x$  (b), sputtered at 10 nbar oxygen partial pressure at room temperature. (c) Comparison of  $V_{2p}$  3/2 peaks recorded for  $VO_x$  and  $(V_{0.9}Cr_{0.1})O_x$  and (d) core level spectra of Chromium Cr 2p.

chosen to ensure a reasonable sensitivity for the Cr-detection. To fit the data, in addition to literature comparison,<sup>12–14</sup> crystalline samples of V, VO,  $V_2O_3$ ,  $VO_2$ , and  $V_2O_5$  were synthesized where oxidation states between +0 and +5 (+1 excluded) could be extracted. These  $V_{2p}$ -binding energies were henceforth taken as reference. Table II summarizes binding energy positions, associated with each oxidation state and used to fit experimental data, as well as integral peak areas of the oxidation states for both samples.

As displayed in Fig. 2, in both cases, every peak of  $V_{2p}$  core level can be decomposed into three elementary components which can be associated with the different oxidation states of vanadium. Starting from lower binding energy, peaks attributed to  $V^{3+}$ ,  $V^{4+}$ , and  $V^{5+}$  oxidation states should be involved to fully fit the recorded spectra. Thus, both samples contain a mix of vanadium valences between +3 and +5 with a major contribution of  $V^{4+}$  at 516.1 eV for the  $V_{2p}$  3/2 peak. In the case of undoped vanadium oxide film, the contributions of  $V^{3+}$  and  $V^{5+}$  are quite similar (29% and 22%, respectively, as displayed in Table II), whereas for the Cr-doped sample the contribution of  $V^{3+}$  significantly increases in comparison to the undoped layer by a factor of 1.5 from 29% to 45% [shown in detail at  $V_{2p}$  3/2 in Fig. 2(c)]. For the Cr-doped layer, the  $V^{3+}$  and  $V^{4+}$  contributions are close together while the  $V^{5+}$  component is less significant at 14%. Considering the Cr 2p core level, chromium appears only oxidized in  $Cr^{3+}$  valence [Fig. 2(d)].

### C. Electrical characterization

At first, undoped  $VO_x$  devices with symmetric Pt-electrodes were investigated [Fig. 3(a)]. After a forming step

(at high voltage and current of at least 7 V and 4 mA, respectively), an apolar volatile threshold switch could be created independently of the applied polarity [Fig. 3(a1)]. The threshold voltage  $V_{ON}$  varied with cycling between 0.1 V up to a maximum voltage of 0.4 V (here shown up to 0.25 V). For temperature dependent  $I$ - $V$  sweeps, the threshold vanished at 60 °C [Fig. 3(a2)]. Such a threshold switch with a broad hysteresis loop is hereby named “TS1”. In Fig. 3(a3), TS1 was formed in a cell at room temperature and afterwards heated up to 70 °C. Then, the pad was cycled with a slow measurement speed in 10 °C steps while cooling down to 10 °C. The OFF-resistance (measured at constant voltage of 20 mV) increased exponentially from 60 °C downwards [as seen in Fig. 3(a4)] and discrete volatile resistance jumps started to form in the  $R$ - $V$  sweeps. The lower the temperature, the more steps were observed. Figure 3(b) depicts  $I$ - $V$  sweeps of an undoped and asymmetric  $VO_x$  device with vanadium as top electrode, which after forming (at a lower voltage of  $\sim 1$  V than symmetric cells) mainly showed bipolar resistive switching (BRS). In very rare cases, asymmetric stacks also showed threshold switching as well as symmetric stacks showed BRS.

Further, symmetric and asymmetric devices with 3 at. % Cr-doped  $VO_x$  films were investigated (Fig. 4). For symmetric devices  $Pt/(V_{0.97}Cr_{0.03})O_x/Pt$  [Fig. 4(a)], it was not possible to induce TS1 or any non-volatile switching. However, a threshold switching, very different from the TS1 of undoped  $VO_x$  films, is systematically observed [Fig. 4(a1)]. Already its forming voltage and current (2.5 V/ less than 1 mA) are indeed lower than for undoped  $VO_x$  (7 V/ 4 mA). Moreover, the threshold occurred at much higher voltage than TS1 (for voltages above 0.6 V instead of 0.25 V for TS1), with narrow or vanishing hysteresis ( $V_{OFF}$  being very close to  $V_{ON}$ ) and without any intermediate steps as shown for the symmetric undoped stack in Fig. 3(a3). Rather, at voltages just before the ON- and after the OFF-switch, the current oscillates right at the transition from high to low resistive state and vice versa [Fig. 4(a2)]. Figures 4(a3) and 4(b1) show these oscillations (within a slow sweep speed) becoming active right

TABLE II. Binding energies and integral peak area for vanadium 2p 3/2 oxidation states +3 +4 and +5 in amorphous  $VO_x$  and  $(V_{0.9}Cr_{0.1})O_x$ .

Oxidation state of vanadium	+3	+4	+5
Binding energy $E_B$ (eV)	515.0 $\pm$ 0.3	516.2 $\pm$ 0.2	517.3 $\pm$ 0.2
Integral peak area (%) undoped	29	49	22
Integral peak area (%) Cr-doped	45	41	14



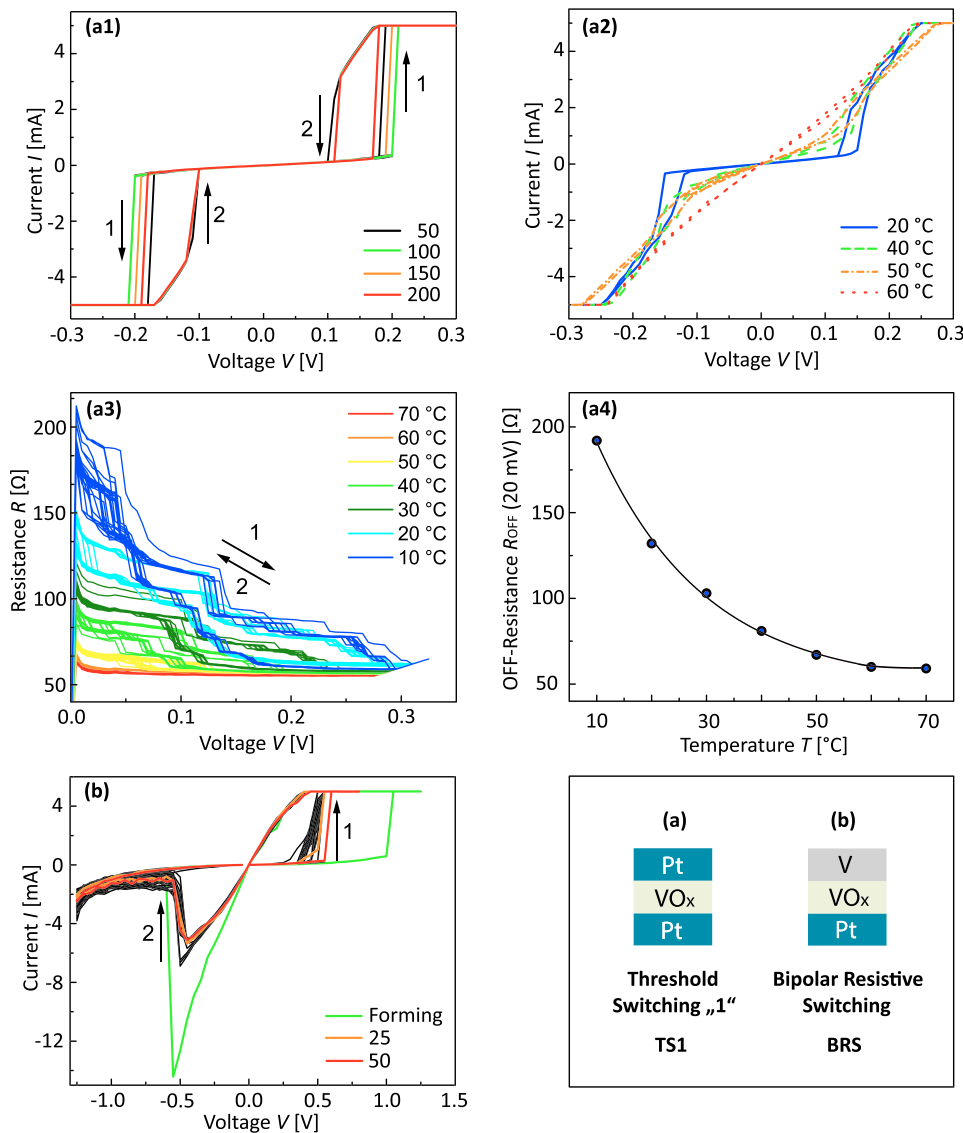


FIG. 3. (a1) After a forming step, symmetric Pt/amorphous VO<sub>x</sub>/Pt shows apolar threshold switching, named “TS1” (with cycle number). Arrows indicate different switching steps: ON-switch (1) and OFF-switch (2) are identical for both polarities. (a2) Quasistatic  $I$ - $V$  measurements in the 20 to 60 °C temperature range: TS1 vanishes at around 60 °C. (a3) Slow sweeps of a cell with TS1 cooling down from 70 °C to 10 °C reveal steps within threshold switching (10 cycles per temperature). Each sweep starts at the high resistance state and switches volatily to lower resistance values with increasing voltage. (a4) OFF-resistance versus temperature with an exponential decay up to 70 °C. (b) Non-volatile bipolar resistive switching for an asymmetric V/amorphous VO<sub>x</sub>/Pt device versus cycle number with ON-switch (1) and OFF-switch (2) (intermediate cycles in black).

after the forming step for symmetric as well as asymmetric stacks. The magnitude of the oscillations increases as the sweep voltage comes closer to the threshold voltage. This kind of threshold switching was also found to be stable in temperature, up to 90 °C [Fig. 4(a1)]. Hence, we categorize this as a different threshold switching mechanism called “TS2”.

For Cr-doped VO<sub>x</sub> devices with asymmetric electrodes, either this new threshold switching TS2 [Fig. 4(b2)] or the VCM-type bipolar non-volatile switching [BRS, Fig. 4(b3)] was randomly found from cell to cell. For the bipolar switching in Fig. 4(b3), a strong non-linearity of the ON-state can be observed, contrary to the behaviour in HfO<sub>2</sub> or Ta<sub>2</sub>O<sub>5</sub> VCM cells at such high current levels in the mA range.<sup>15</sup>

In general, Cr-doped symmetric devices showed a higher OFF-resistance (Table III) compared to undoped devices. Where asymmetric devices revealed a comparable OFF-resistance independent of doping, for undoped devices, the ON-state was clearly ohmic with a smaller resistance of about one order of magnitude compared to doped devices.

## IV. DISCUSSION

### A. Influence of chromium doping on layer morphology and stoichiometry

Undoped as well as Cr-doped samples were classified as X-ray amorphous as verified by XRD:GI analysis. Apart from filament crystallinity, as shown in Secs. III A and III B, considerable differences have been found between undoped and Cr-doped sputtered VO<sub>x</sub> thin films concerning vanadium valence states, density, and morphology.

For undoped VO<sub>x</sub>, a major V<sup>4+</sup> valence contribution is found [Fig. 2(a)]. Taking into account the sputtering conditions (process pressure of 10 μbar and a substrate-to-melting temperature ratio to VO<sub>2</sub> (1967 °C) of  $\frac{T_s}{T_{m,VO_2}} = 0.134$ ), the Thornton model<sup>16</sup> would predict a porous amorphous structure named “Zone 1”. This morphology has indeed been observed [Figs. 1(a) and 1(b)] for VO<sub>x</sub> and is supported by the determined density (4.0 g/cm<sup>3</sup>) that is close (85%) to the theoretical crystalline density of VO<sub>2</sub> [4.69 g/cm<sup>3</sup> (Ref. 17)].

In the case of Cr-doped VO<sub>x</sub> obtained by cosputtering, the investigated physical properties change. Referring to the core level spectrum of vanadium [Fig. 2(c)], with Cr-doping,

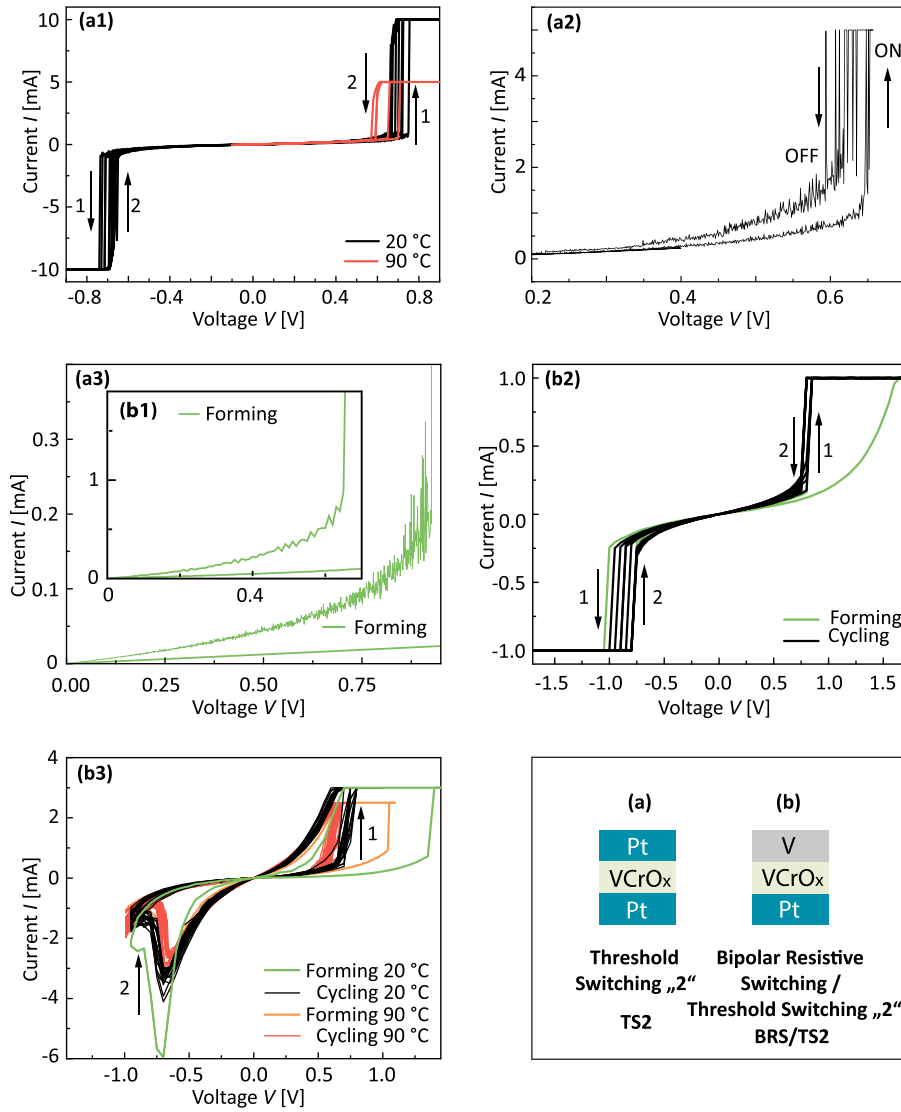


FIG. 4. (a1) Symmetric Pt/(V<sub>0.97</sub>Cr<sub>0.03</sub>)O<sub>x</sub>/Pt stack with volatile switching called “TS2”. Arrows indicate different switching steps: ON-switch (1) and OFF-switch (2). (a2) Current Oscillations at the threshold voltage in ON- and OFF-switch. [(a3) and (b1)] Current oscillations occur only after forming of the threshold switch (measured with slow sweep speed) in a symmetric and an asymmetric stack. (b2) Analogue volatile switching in an asymmetric V/(V<sub>0.97</sub>Cr<sub>0.03</sub>)O<sub>x</sub>/Pt stack. (b3) Bipolar resistive switching “BRS” in an asymmetric stack. Note about the different used current compliances (“CC”): (i) the high CCs in (a1), (10 mA for 20 °C, 5 mA at 90 °C) were applied to reveal the ON-state (sloped region); (ii) for the asymmetric stacks, limiting the CC to 1 mA was required to obtain pure TS (b2) while higher CC resulted in BRS (b3).

the integral  $V_{2p} 3/2$  binding energy shifts to lower values which results in a higher relative contribution of  $V^{3+}$  (Table II). Since  $Cr^{3+}$  is the most stable oxidation state of chromium [as well as the only oxidation state recorded in our samples, see Fig. 2(d)] and  $Cr_2O_3$  having the same rutile  $R\bar{3}c$  structure as  $V_2O_3$ , chromium could impose and stabilize a corundum-like near neighbour preorientation and therefore force a higher relative amount of  $V^{3+}$  inside the grains. Further, the higher density value of  $4.4 \text{ g/cm}^3$  for Cr-doped thin films (V<sub>0.97</sub>Cr<sub>0.03</sub>)O<sub>x</sub> is in agreement with the observed compact oriented columnar growth of grains which is typically obtained in the co-sputtering mode.<sup>18</sup> With doping, the morphology now matches “Zone T” of the Thornton model for the same sputter conditions instead of Zone 1 for VO<sub>x</sub>.

TABLE III. Resistance at a voltage of 0.1 V for different devices and resistive switching states.

Resistance $R$ (k $\Omega$ ) (0.1V)	Undoped	3 at. % Cr-doped
Symmetric OFF	0.2–0.9	3–3.8
Asymmetric OFF	4–5	3–5
Asymmetric ON	0.05–0.07	0.54–0.62

The density of our Cr-doped VO<sub>x</sub> is similarly close (87%) to the density of crystalline V<sub>2</sub>O<sub>3</sub> ( $5.03 \text{ g/cm}^3$ );<sup>20</sup> less oxygen rich phases such as V<sub>2</sub>O<sub>3</sub> possess higher densities than VO<sub>2</sub>.<sup>19</sup>

This compact structure should also have a stabilizing influence on the reliability of Cr-doped devices by preventing inclusion of impurities or moisture which could subsequently alter the oxidation state of vanadium.<sup>21</sup>

## B. Interpretation of the different threshold switching modes (TS1, TS2)

### 1. Threshold TS1

As seen in Figs. 3(a2) and 3(a3), the nature of the TS1 threshold is evidenced by determining the transition temperature from  $I$ – $V$  measurements as function of temperature. The so-called TS1 vanishes slightly above 60 °C with the sample becoming ohmic. This dependence makes the threshold very likely to be caused by the temperature driven IMT in crystalline VO<sub>2</sub>. Since our pristine oxidation state is dominated by  $V^{4+}$  valence, it is reasonable to conclude that local crystallization to VO<sub>2</sub> can be triggered by the forming step. The switching characteristics [Fig. 3(a)] including hysteresis

and intermediate steps match well a thermally triggered transition with an S-type negative differential resistance.<sup>22,23</sup> In the case of thermal cycling of VO<sub>2</sub>, resistance jumps have equally been reported<sup>24</sup> and are in good agreement with our electrical measurements. These jumps were explained by a series of avalanches in the coexistence regime of metallic and insulating phases of VO<sub>2</sub>. Additional analysis of the TS1 switching is presented in Fig. 5(a). By subtracting the series resistance effect, the device resistance switches between two constant resistance values ( $R_{\text{OFF}}$  and  $R_{\text{ON}}$ ), with the power at ON switching (point 1) matching that at OFF switching (point 2) [Fig. 5(a3)]. This analysis further evidences that TS1 is caused by a thermally induced IMT.

## 2. Threshold TS2

The second threshold mechanism only occurred in Cr-doped stacks [Figs. 4(a) and 4(b)]. In addition, it occurs for threshold voltages far above the investigated (V,Cr)O<sub>2</sub>, namely, in the range of 0.6 V up to 1.2 V, depending on the applied current compliance and stack symmetry. (V,Cr)O<sub>2</sub> can definitely be excluded due to the fact that the threshold still persists over 90 °C (Fig. 4(a1) red curve). It could be speculated that this TS2 is associated with the presence of

V<sub>3</sub>O<sub>5</sub> which exhibits an IMT above 90 °C, namely, at 155 °C<sup>4</sup> associated with a crystallographic phase change. Further analysis of TS2, however, is evidencing the very different nature of TS2 compared to TS1 [Fig. 5(b)] which excludes a temperature driven crystallographic phase change such as in V<sub>3</sub>O<sub>5</sub>. Where TS1 switches between two constant resistance states  $R_{\text{OFF}}$  and  $R_{\text{ON}}$ , TS2 (after correction for a series resistance) switches between  $R_{\text{OFF}}$  and a second state with zero dynamic resistance [Fig. 5(b1)]. This kind of switching is not compatible with a thermal IMT but indicative of an electronically induced filamentary switching process as that observed in Cr-doped V<sub>2</sub>O<sub>3</sub>.<sup>10</sup> OFF switching is hereby induced not by a power condition but by a minimum required holding current [Figs. 5(b2) and 5(b3)]. In this case, the OFF switch power (at the minimum holding current) is 5–10 times higher than the ON switch power, further evidencing it not to be a temperature induced transition (in spite of the temperature dependence of the holding current itself). In principle, such electronically induced threshold switching can occur even for amorphous materials and so would not depend on the presence of a special crystalline material phase. The requirement of an initial forming step and the evidence that for the case of undoped films, this

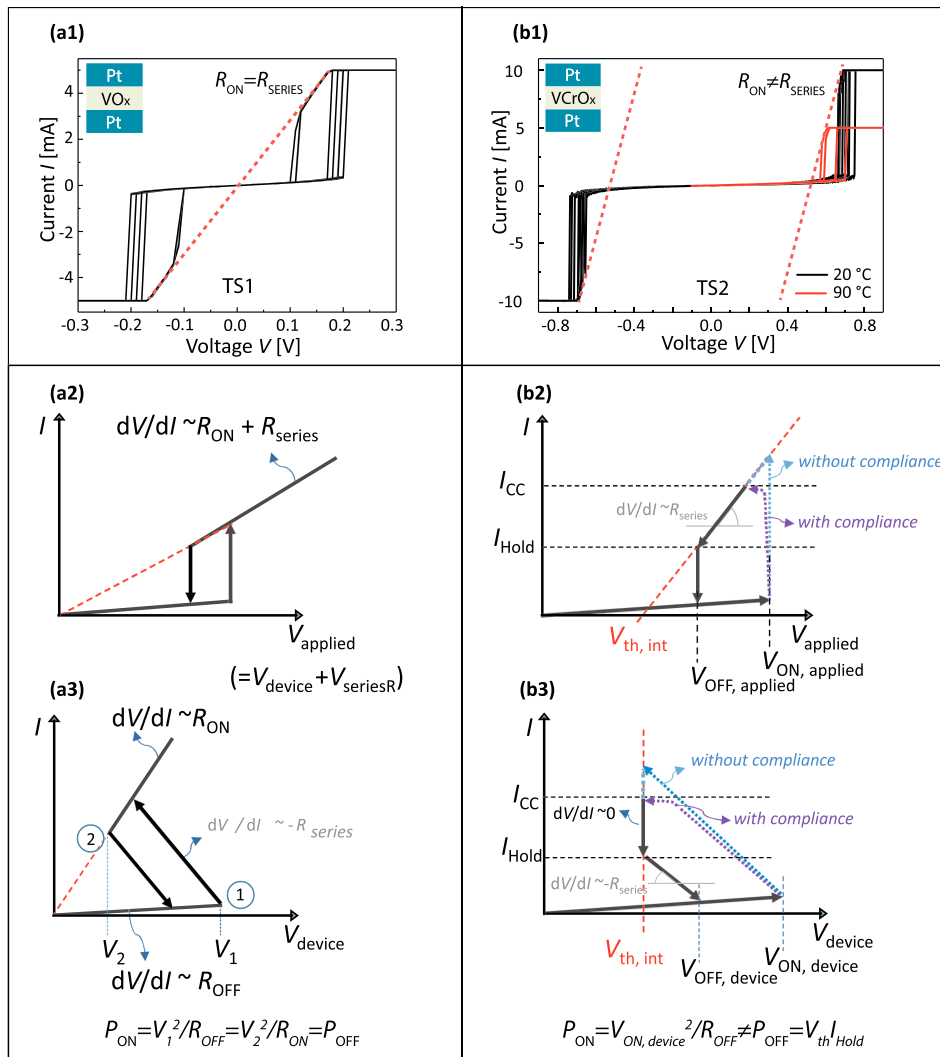


FIG. 5. Analysis of typical TS1 and TS2 behavior. The positive and negative bias ON state of TS1 for the undoped symmetric device shows a single linear  $I$ - $V$  characteristic that goes through the origin when extrapolated (Fig. 5(a1) dashed line). Based on a power analysis (see [supplementary material](#), S2), the intrinsic TS1 characteristic of the device [by subtracting the voltage drop over the series resistance, see Figs. 5(a2) and 5(a3)] is consistent with a temperature induced IMT. The positive and negative bias ON state of TS2 (for the Cr-doped symmetric device) shows two symmetric  $I$ - $V$  characteristics that cross the voltage axis at voltages  $+V_{\text{th,int}}$  and  $-V_{\text{th,int}}$  of  $\pm 0.5$  V (Fig. 5(b1) dashed line). By subtracting the voltage drop over the series resistance [Fig. 5(b2)], the intrinsic device characteristic can be derived [Fig. 5(b3)]. This characteristic, with intrinsic vertical  $I$ - $V$  at  $V_{\text{th}}$  and a minimum holding current, is typical for an electronic induced filamentary threshold switching (the properties of the filament in thickness and/or conductivity adapt to the current to result in a zero dynamic resistance).

results in the formation of a crystalline ( $\text{VO}_2$ ) phase, however, strongly suggest that also here we probably form a crystalline phase, which then cannot stem from a phase showing a thermal IMT as  $\text{VO}_2$ . In addition, the strong current oscillations jumping back and forth (right at the threshold voltage) can be explained by a metastable conductive filament as result of an electronically induced Mott-transition.<sup>10</sup> There, a persisting competition arises between an electrically triggered conductive path and—by associated Joule heating—a thermally induced relaxation of metallic domains to an insulating state. This is in strong contrast to a Joule-heating driven transition to a conductive state in  $\text{VO}_2$  (or  $\text{V}_3\text{O}_5$ ) with each conductive jump arising one after the other solely towards further ON-switch (increasing voltage) or further OFF-switch (decreasing voltage).

For these reasons, we clearly favour the explanation according to which TS2 is related to the presence of a crystalline  $(\text{V}_{0.97}\text{Cr}_{0.03})_2\text{O}_3$  Mott phase.

### C. Device model

Forming in metal-oxide based ReRAM structures is generally considered to be a two-step process.<sup>25</sup> First, a purely electronic conduction path is initiated by dielectric breakdown. Second, the strong Joule heating due to the highly localized current leads to high local temperatures<sup>26,27</sup> and typically induces more permanent material changes like atomic/ionic migration and phase changes [Fig. 6(a)]. For instance, defects like oxygen vacancies can be created and/or drift in the existing electrical field. This will thus lead to strong changes of local oxygen stoichiometry, resulting in a filamentary oxygen vacancy cluster or even the formation of crystalline suboxide phases [Fig. 6(b)] similarly to the creation of Magnéli phases reported in  $\text{TiO}_x$  films.<sup>28</sup> Concomitantly, a high electronic conductivity may locally arise due to the doping effect of the oxygen vacancies (i.e., valence change effect), or more directly by the electronic conductivity of formed suboxide crystalline phases.

In Sec. IV B, we explained the observed threshold switching characteristics by the presence of specific crystalline phases controlling the current. This, however, does not preclude the co-presence of other phases inside the filament. Indeed, many stable crystalline Magnéli phases between  $\text{V}_2\text{O}_3$  and  $\text{VO}_2$  exists and so may be expected to form as well (all possess a rutile based structure with only a difference in crystallographic shear planes in the oxygen sublattice). However, all known (undoped) crystalline phases in this valency range show metallic behaviour at room temperature,<sup>2</sup> so they are not expected to control the current as observed by  $I$ - $V$ -sweeps.

#### 1. Symmetric devices $\text{Pt}/\text{VO}_x/\text{Pt}$

For the symmetric devices with undoped  $\text{VO}_x$  films  $\text{Pt}/\text{VO}_x/\text{Pt}$ , we showed by temperature measurements that a crystalline  $\text{VO}_2$  phase is very likely to be formed as a current-controlling part of the conductive filament where the complete filament may be composite of this phase together with other conducting suboxide crystalline phases and/or

domains with oxygen vacancies [Fig. 6(b)]. This  $\text{VO}_2$  phase induces the (TS1) threshold switching when the filament temperature is raised above  $68^\circ\text{C}$  (the IMT temperature of  $\text{VO}_2$ ) by Joule heating [Fig. 6(c)].

#### 2. Symmetric devices $\text{Pt}/(\text{V,Cr})\text{O}_x/\text{Pt}$

For the Cr-doped  $\text{VO}_x$  based symmetric devices  $\text{Pt}/(\text{V,Cr})\text{O}_x/\text{Pt}$ , we expect a similar filament consisting of crystalline phase(s). However, we hypothesize that the higher  $\text{V}^{3+}$  content associated with the presence of  $\text{Cr}^{3+}$  [see Fig. 2(d)] favours the formation of a  $(\text{V}_{0.97}\text{Cr}_{0.03})_2\text{O}_3$  phase rather than a  $(\text{V}_{0.97}\text{Cr}_{0.03})\text{O}_2$  phase.

Therefore, we observe a different threshold behaviour named TS2 instead of TS1 which appears to be solely triggered by an electronic process. The intrinsic threshold field of our observed process ( $\sim 60\text{ kV/cm}$ ) is 10 times higher than reported for electronic avalanche process in the same material for single crystals ( $\sim 6\text{ kV/cm}$ ).<sup>29</sup> Therefore, other electronic mechanisms could also explain triggering the transition in our thin films such as Landau-Zener quantum tunnelling through the Mott-Hubbard gap ( $10^2$ – $10^3\text{ kV/cm}$ ) where self-induced current oscillations were also reported as result of a numerical analysis.<sup>30</sup>

Apart from the actual mechanism, the difference between the field values in the thick crystal samples and our films may also be indicative of an interfacial process (with most of the voltage drop over the interface, resulting in a non-realistic homogenous field calculation).

#### 3. Asymmetric undoped and Cr-doped $\text{VO}_x$

Finally, for the asymmetric devices, oxygen scavenging by the vanadium electrode results in lower oxygen content within the thin film. This is likely to inhibit the formation of (especially higher oxygen content) threshold switching phases as  $\text{VO}_2$  and to a lesser effect, even of  $(\text{V}_{0.97}\text{Cr}_{0.03})_2\text{O}_3$ . Such assumptions are in good agreement with (i) the observation of only BRS in asymmetric  $\text{VO}_x$  devices and (ii) observation of a BRS or a TS2 behaviour in asymmetric  $(\text{V}_{0.97}\text{Cr}_{0.03})\text{O}_x$  devices. Interestingly, Singh *et al.*<sup>31</sup> observed both BRS and a TS in asymmetric  $\text{Pt}/\text{VO}_x/\text{Ti}$  devices using high oxygen content ( $\text{V}:\text{O}=1:2$ – $2:5$ ) undoped amorphous  $\text{VO}_x$  films deposited by Atomic Layer Deposition (ALD). The threshold switch they observed has the characteristics of our TS1 and was also associated with the formation of a  $\text{VO}_2$  IMT phase. In their case, the oxygen scavenging by the titanium electrode apparently did not prevent the formation of  $\text{VO}_2$  because of the initial much higher oxygen content in the as-deposited films.

While in typical BRS switching cells (as made out of  $\text{HfO}_2$ ), the filament is expected to exist out of a dense cluster of oxygen vacancy defects, in view of the many different existing  $\text{V}_z\text{Cr}_y\text{O}_x$  material phases, we may expect the creation of other, lower O-content, conducting crystalline material phases inside the filament as  $\text{V}_4\text{O}_7$  or  $\text{V}_8\text{O}_{15}$ . As most of these phases only show a possible IMT transition at low temperatures far below room temperature,<sup>2</sup> the only resistive switching mechanism observed is a non-volatile BRS. The high non-linearity of the ON-state at rather high current levels [Fig. 4(b3)] may indeed be an indication of a suboxide



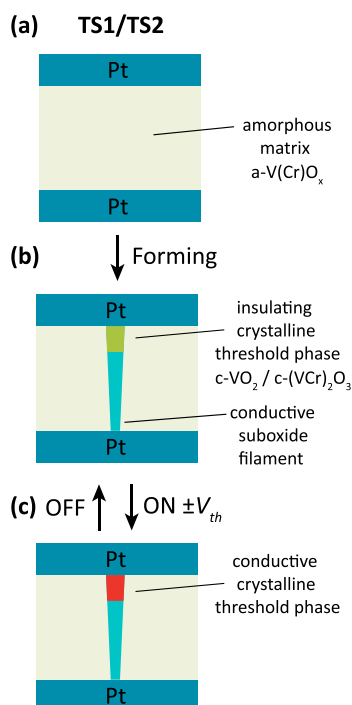


FIG. 6. Device model for symmetric undoped and Cr-doped devices. Before a forming step (a) an amorphous matrix is present. After forming (b), a filament is created which may consist of conductive metallic suboxide phases in a plug, combined with a current controlling disc which is responsible for threshold switching (c), either through a temperature-induced MIT with  $\text{VO}_2$  or an electronic transition in Cr-doped  $\text{V}_2\text{O}_3$ .

crystalline phase.<sup>32</sup> Metal oxide phases without stable suboxide phases (e.g.,  $\text{HfO}_2$ ) show a very linear ON state conduction above  $50\ \mu\text{A}$ ,<sup>15</sup> while  $\text{TiO}_2$  that also forms different suboxides shows a strong ON state non-linearity as well.<sup>33</sup>

## V. CONCLUSION

Resistive switching was investigated in undoped and Cr-doped amorphous vanadium oxide layers synthesized by low temperature reactive sputtering at a very low oxygen partial pressure in the nanobar regime. For all films and symmetric devices with Pt as top and bottom electrode and after a forming step, a volatile threshold switching was observed. For undoped films, this threshold switching is associated with the insulator to metal transition (IMT) in a  $\text{VO}_2$  phase created in the filament generated by electrical means and disappears above  $60^\circ\text{C}$ . For Cr-doped films, a different threshold switching behaviour appears being stable up to  $90^\circ\text{C}$ . The different switching characteristics are indicative of an electronic rather than temperature induced transition, thus associated with an electronic induced Mott transition in  $(\text{V}_{0.97}\text{Cr}_{0.03})_2\text{O}_3$ . Cr doping is indeed found to increase the occurrence of  $\text{V}^{3+}$  oxidation state in as-deposited film, which may favour the local formation of such Mott phase during the forming step. For asymmetric devices with platinum bottom electrode and vanadium top electrode, the oxygen scavenging action of the vanadium reduces the oxygen content within the film, inhibiting the formation of these (higher oxygen content) threshold switching phases and consequently favouring the occurrence of classical VCM type

bipolar switching based on the drift of oxygen vacancies. Due to their high temperature stability, these new Mott-based  $\text{Pt}/(\text{V,Cr})\text{O}_x/\text{Pt}$  threshold switching devices may be of high interest for new ReRAM crossbar selector devices. While further optimization of the device (e.g., Cr-doping) is required to meet the application requirements of high ON/OFF ratio and low OFF current operation, the use of amorphous films instead of crystalline films offers the huge advantage of a better back-end process compatibility due to the high ( $\sim 600^\circ\text{C}$ ) deposition temperature required for depositing well crystallized films while also the OFF resistance of crystalline devices is lower than that of amorphous ones.<sup>34</sup>

## SUPPLEMENTARY MATERIAL

See [supplementary material](#) for the comments on the calculation of the chromium content of cosputtered samples by XPS analysis (Table S1). Further, a power analysis (S2) is given for the two observed volatile switching modes (Fig. 5) to distinguish between a pure thermally induced insulator-to-metal transition and one typical for an electronically induced filamentary switching process.

## ACKNOWLEDGMENTS

J. A. J. Rupp would like to thank M. Rose and G. C. Huang for the support in sample preparation and measurement, K. Skaja, C. Bäumer, D. Bick, and C. Rosário for the discussion of XPS and switching results and L. Cario, B. Corraze, and J. Tranchant (IMN, University of Nantes) for fruitful discussions. Furthermore, J. A. J. Rupp greatly acknowledges the Deutsche Forschungsgemeinschaft DFG for funding this project in the Sonderforschungsbereich (SFB) 917.

<sup>1</sup>H. A. Wriedt, *Bull. Alloy Phase Diagrams* **10**, 271 (1989).

<sup>2</sup>A. L. Pergament, G. B. Stefanovich, N. A. Kuldin, and A. A. Velichko, *ISRN Condens. Matter Phys.* **960627**, 2013 (2013).

<sup>3</sup>F. J. Morin, *Phys. Rev. Lett.* **3**, 34 (1959).

<sup>4</sup>L. Baldassarre, A. Perucchi, E. Arcangeletti, D. Nicoletti, D. Di Castro, P. Postorino, V. A. Sidorov, and S. Lupi, *Phys. Rev. B* **75**, 245108 (2007).

<sup>5</sup>M. Son, J. Lee, J. Park, J. Shin, G. Choi, S. Jung, W. Lee, S. Kim, S. Park, and H. Hwang, *IEEE Electron Device Lett.* **32**, 1579 (2011).

<sup>6</sup>F. A. Chudnovskii, L. L. Olynets, A. L. Pergament, and G. B. Stefanovich, *J. Solid State Chem.* **122**, 95 (1996).

<sup>7</sup>B. L. Brown, M. Lee, P. G. Clem, C. D. Nordquist, T. S. Jordan, S. L. Wolfley, D. Leonhardt, C. Edney, and J. A. Custer, *J. Appl. Phys.* **113**, 173704 (2013).

<sup>8</sup>C. Funck, S. Menzel, N. Aslam, H. Zhang, A. Hardtdegen, R. Waser, and S. Hoffmann-Eifert, *Adv. Electron. Mater.* **2**, 1600169 (2016).

<sup>9</sup>D. B. McWhan, T. M. Rice, and J. P. Remeika, *Phys. Rev. Lett.* **23**, 1384 (1969).

<sup>10</sup>E. Janod, J. Tranchant, B. Corraze, M. Querré, P. Stoliar, M. Rozenberg, T. Cren, D. Roditchev, V. T. Phuoc, M. P. Besland, and L. Cario, *Adv. Funct. Mater.* **25**, 6287 (2015).

<sup>11</sup>R. Waser, R. Dittmann, G. Staikov, and K. Szot, *Adv. Mater.* **21**, 2632 (2009).

<sup>12</sup>G. Silversmit, D. Depla, H. Poelman, G. B. Marin, and R. De Gryse, *J. Electron. Spectrosc. Relat. Phenom.* **135**, 167 (2004).

<sup>13</sup>M. C. Biesinger, L. W. M. Lau, A. R. Gerson, and R. St. C. Smart, *App. Surf. Sci.* **257**, 887 (2010).

<sup>14</sup>M. Demeter, M. Neumann, and W. Reichelt, *Surf. Sci.* **454–456**, 41 (2000).

<sup>15</sup>A. Fantini, D. J. Wouters, R. Degraeve, L. Goux, L. Pantisano, G. Kar, Y.-Y. Chen, B. Govoreanu, J. A. Kittl, L. Altissimi, and M. Jurczak, in *Proceedings of the 4th IEEE International Memory Workshop (IMW)* (2012), pp. 1–4.

- <sup>16</sup>J. A. Thornton, *J. Vac. Sci. A* **4**, 3059 (1986).
- <sup>17</sup>G. Andersson, *Acta Chem. Scand.* **8**, 1599 (1954). ICCD: 00-009-0142.
- <sup>18</sup>M. Querré, E. Janod, L. Cario, J. Tranchant, B. Corraze, V. Bouquet, S. Deputier, S. Cordier, M. Guilloux-Viry, and M.-P. Besland, *Thin Solid Films* **617**, 56–62 (2016).
- <sup>19</sup>B. D. Gauntt, Ph.D. thesis (Pennsylvania State University, 2011), p. 19.
- <sup>20</sup>M. C. Morris, H. F. McMurdie, E. H. Evans, B. Paretkin, H. S. Parker, and N. C. Panagiotopoulos, Natl. Bur. Stand. (U.S.) Monogr. 25 **20**, 108 (1981). ICCD: 00-034-0187.
- <sup>21</sup>G. H. Kelsall, I. Thompson, and P. A. Francis, *J. Appl. Electrochem.* **23**, 417 (1993).
- <sup>22</sup>A. Pergament, G. Stefanovich, V. Malinenko, and A. Velichko, *Adv. Condens. Matter Phys.* **2015**, 654840.
- <sup>23</sup>C. Ko and S. Ramanathan, *Appl. Phys. Lett.* **93**, 252101 (2008).
- <sup>24</sup>A. Sharoni, J. G. Ramirez, and I. K. Schuller, *Phys. Rev. Lett.* **101**, 026404 (2008).
- <sup>25</sup>A. Sharma, M. Noman, M. Abdelmoula, M. Skowronski, and J. A. Bain, *Adv. Funct. Mater.* **24**, 5522 (2014).
- <sup>26</sup>S. Menzel, M. Waters, A. Marchewka, U. Boettger, R. Dittmann, and R. Waser, *Adv. Funct. Mater.* **21**, 4487 (2011).
- <sup>27</sup>B. Govoreanu, S. Clima, I. Radu, Y. Chen, D. Wouters, and M. Jurczak, *IEEE Trans. Electron Devices* **60**, 2471 (2013).
- <sup>28</sup>D.-H. Kwon, K. M. Kim, J. H. Jang, J. M. Jeon, M. H. Lee, G. H. Kim, X.-S. Li, G.-S. Park, B. Lee, S. Han, M. Kim, and C. S. Hwang, *Nat. Nanotechnol.* **5**, 148 (2010).
- <sup>29</sup>P. Stoliar, L. Cario, E. Janod, B. Corraze, C. Guillot-Deudon, S. Salmon-Bourmand, V. Guiot, J. Tranchant, and M. Rozenberg, *Adv. Mater.* **25**, 3222 (2013).
- <sup>30</sup>T. Oka, R. Arita, and H. Aoki, *Phys. Rev. Lett.* **91**, 066406 (2003).
- <sup>31</sup>T. Singh, S. Wang, N. Aslam, H. Zhang, S. Hoffmann-Eifert, and S. Mathur, *Chem. Vap. Depos.* **20**, 291–297 (2014).
- <sup>32</sup>J. Woo, S. Kim, W. Lee, D. Lee, S. Park, G. Choi, E. Cha, and H. Hwang, *Appl. Phys. Lett.* **102**, 112115 (2013).
- <sup>33</sup>F. Lentz, B. Roesgen, V. Rana, D. J. Wouters, and R. Waser, *IEEE Electron Device Lett.* **34**, 996 (2013).
- <sup>34</sup>J. A. J. Rupp, R. Waser, and D. J. Wouters, in Proceedings of the 8th IEEE International Memory Workshop (IMW) (2016), pp. 37–40.